Eur. Phys. J. C (2023) 83:344
https://doi.org/10.1140/epjc/s10052-023-11401-5

THE EUROPEAN PHYSICAL JOURNAL C

Regular Article - Experimental Physics

First observation of the cosmic ray shadow of the Moon and the Sun with KM3NeT/ORCA

S. Aiello[1], A. Albert[2,56], S. Alves Garre[3], Z. Aly[4], A. Ambrosone[5,6], F. Ameli[7], M. Andre[8], M. Anghinolfi[9], M. Anguita[10], M. Ardid[11], S. Ardid[11], J. Aublin[12], C. Bagatelas[13], L. Bailly-Salins[14], B. Baret[12], S. Basegmez du Pree[15], Y. Becherini[12], M. Bendahman[12,16], F. Benfenati[17,18], E. Berbee[15], V. Bertin[4], S. Biagi[19], M. Boettcher[20], M. Bou Cabo[21], J. Boumaaza[16], M. Bouta[22], M. Bouwhuis[15], C. Bozza[23], H. Brânzaş[24], R. Bruijn[15,25], J. Brunner[4,a], R. Bruno[1], E. Buis[15,26], R. Buompane[5,27], J. Busto[4], B. Caiffi[9], D. Calvo[3], S. Campion[7,28], A. Capone[7,28], F. Carenini[7,28], V. Carretero[3], P. Castaldi[17,29], S. Celli[7,28], L. Cerisy[4,b], M. Chabab[30], N. Chau[12], A. Chen[31], R. Cherkaoui El Moursli[16], S. Cherubini[19,32], V. Chiarella[33], T. Chiarusi[17], M. Circella[34], R. Cocimano[19], J. A. B. Coelho[12], A. Coleiro[12], R. Coniglione[19], P. Coyle[4], A. Creusot[12], A. Cruz[35], G. Cuttone[19], R. Dallier[36], Y. Darras[37], A. De Benedittis[5], B. De Martino[4], R. Del Burgo[5], I. Di Palma[7,28], A. F. Dìaz[10], D. Diego-Tortosa[11], C. Distefano[19], A. Domi[15,25], C. Donzaud[12], D. Dornic[4], M. Dörr[38], E. Drakopoulou[13], D. Drouhin[2,56], T. Eberl[37], A. Eddyamoui[16], T. van Eeden[15], M. Eff[37], D. van Eijk[15], I. El Bojaddaini[22], S. El Hedri[12], A. Enzenhöfer[4], V. Espinosa[11], G. Ferrara[19,32], M. D. Filipović[39], F. Filippini[17,18], L. A. Fusco[5,40], J. Gabriel[41], T. Gal[37], J. García Méndez[11], A. Garcia Soto[3], F. Garufi[5,6], C. Gatius Oliver[15], N. Geißelbrecht[37], L. Gialanella[5,27], E. Giorgio[19], A. Girardi[7], I. Goos[12], S. R. Gozzini[3], R. Gracia[37], K. Graf[37], D. Guderian[57], C. Guidi[9,42], B. Guillon[14], M. Gutiérrez[43], L. Haegel[12], H. van Haren[44], A. Heijboer[15], A. Hekalo[38], L. Hennig[37], J. J. Hernández-Rey[3], F. Huang[4], W. Idrissi Ibnsalih[5,27], G. Illuminati[17,18], C. W. James[35], D. Janezashvili[45], M. de Jong[15,46], P. de Jong[15,25], B. J. Jung[15], P. Kalaczyński[47], O. Kalekin[37], U. F. Katz[37], N. R. Khan Chowdhury[3], G. Kistauri[45], F. van der Knaap[26], P. Kooijman[25,58], A. Kouchner[12,48], V. Kulikovskiy[9], M. Labalme[14], R. Lahmann[37], A. Lakhal[12], M. Lamoureux[12,59], G. Larosa[19], C. Lastoria[4], A. Lazo[3], R. Le Breton[12], S. Le Stum[4], G. Lehaut[14], E. Leonora[1], N. Lessing[37], G. Levi[17,18], S. Liang[12], M. Lindsey Clark[12], F. Longhitano[1], L. Maderer[12], J. Majumdar[15], J. Mańczak[3], A. Margiotta[17,18], A. Marinelli[5], C. Markou[13], L. Martin[36], J. A. Martínez-Mora[11], A. Martini[33], F. Marzaioli[5,27], M. Mastrodicasa[49], S. Mastroianni[5], K. W. Melis[15], S. Miccichè[19], G. Miele[5,6], P. Migliozzi[5], E. Migneco[19], P. Mijakowski[47], C. M. Mollo[5], L. Morales-Gallegos[5], C. Morley-Wong[35], A. Moussa[22], R. Muller[15], M. R. Musone[5], M. Musumeci[19], L. Nauta[15], S. Navas[43], C. A. Nicolau[7], B. Nkosi[31], B. Ó. Fearraigh[15,25], A. Orlando[19], E. Oukacha[12], J. Palacios González[3], G. Papalashvili[45], R. Papaleo[19], E. J. Pastor Gomez[3], A. M. Păun[24], G. E. Păvălaş[24], C. Pellegrino[18,60], S. Peña Martínez[12], M. Perrin-Terrin[4], J. Perronnel[14], V. Pestel[15,25], P. Piattelli[19], O. Pisanti[5,6], C. Poirè[11], V. Popa[24], T. Pradier[2], S. Pulvirenti[19], G. Quéméner[14], U. Rahaman[3], N. Randazzo[1], S. Razzaque[50], I. C. Rea[5], D. Real[3], S. Reck[37], G. Riccobene[19], J. Robinson[20], A. Romanov[9,42], F. Salesa Greus[3], D. F. E. Samtleben[15,46], A. Sánchez Losa[3,34], M. Sanguineti[9,42], C. Santonastaso[5,51], D. Santonocito[19], P. Sapienza[19], A. Sathe[37], J. Schnabel[37], M. F. Schneider[37], J. Schumann[37], H. M. Schutte[20], J. Seneca[15], I. Sgura[34], R. Shanidze[45], A. Sharma[52], A. Simonelli[5], A. Sinopoulou[13], M. V. Smirnov[37], B. Spisso[5,40], M. Spurio[17,18], D. Stavropoulos[13], S. M. Stellacci[5,40], M. Taiuti[9,42], K. Tavzarashvili[53], Y. Tayalati[16], H. Tedjditi[9], H. Thiersen[20], S. Tsagkli[13], V. Tsourapis[13], E. Tzamariudaki[13], V. Van Elewyck[12,48], G. Vannoye[4], G. Vasileiadis[54], F. Versari[17,18], S. Viola[19], D. Vivolo[5,27], H. Warnhofer[37], J. Wilms[55], E. de Wolf[15,25], H. Yepes-Ramirez[11], T. Yousfi[22], S. Zavatarelli[9], A. Zegarelli[7,28], D. Zito[19], J. D. Zornoza[3], J. Zúñiga[3], N. Zywucka[20]

[1] INFN, Sezione di Catania, Via Santa Sofia 64, 95123 Catania, Italy
[2] Université de Strasbourg, CNRS, IPHC UMR 7178, 67000 Strasbourg, France
[3] IFIC-Instituto de Física Corpuscular (CSIC-Universitat de València), c/Catedrático José Beltrán, 2, 46980 Paterna, Valencia, Spain
[4] Aix Marseille Univ, CNRS/IN2P3, CPPM, Marseille, France
[5] INFN, Sezione di Napoli, Complesso Universitario di Monte S. Angelo, Via Cintia ed. G, 80126 Napoli, Italy

[6] Dip. Scienze Fisiche "E. Pancini", Complesso Universitario di Monte S. Angelo, Università di Napoli "Federico II", Via Cintia ed. G, 80126 Napoli, Italy
[7] INFN, Sezione di Roma, Piazzale Aldo Moro 2, 00185 Roma, Italy
[8] Laboratori d'Aplicacions Bioacústiques, Centre Tecnològic de Vilanova i la Geltrú, Universitat Politècnica de Catalunya, Avda. Rambla Exposició, s/n, 08800 Vilanova i la Geltrú, Spain
[9] INFN, Sezione di Genova 33, Genova 16146, Italy
[10] Department of Computer Architecture and Technology/CITIC, University of Granada, 18071 Granada, Spain
[11] Instituto de Investigación para la Gestión Integrada de las Zonas Costeras, Universitat Politècnica de València, C/ Paranimf, 1, 46730 Gandia, Spain
[12] Université de Paris, CNRS, Astroparticule et Cosmologie, 75013 Paris, France
[13] NCSR Demokritos, Institute of Nuclear and Particle Physics, Ag. Paraskevi Attikis, 15310 Athens, Greece
[14] LPC CAEN, A02182036, 6 boulevard Maréchal Juin, 14050 Caen, France
[15] Nikhef, National Institute for Subatomic Physics, PO Box 41882, 1009 DB Amsterdam, The Netherlands
[16] University Mohammed V in Rabat, Faculty of Sciences, 4 av. Ibn Battouta, B.P. 1014, 10000 Rabat, Morocco
[17] INFN, Sezione di Bologna, v.le C. Berti-Pichat, 6/2, 40127 Bologna, Italy
[18] Dipartimento di Fisica e Astronomia, Università di Bologna, v.le C. Berti-Pichat, 6/2, 40127 Bologna, Italy
[19] INFN, Laboratori Nazionali del Sud, Via S. Sofia 62, 95123 Catania, Italy
[20] Centre for Space Research, North-West University, Private Bag X6001, Potchefstroom 2520, South Africa
[21] Instituto Español de Oceanografía, Unidad Mixta IEO-UPV, C/ Paranimf, 1, 46730 Gandia, Spain
[22] University Mohammed I, Faculty of Sciences, Mohammed VI, B.V. 717, R.P. 60000 Oujda, Morocco
[23] Dipartimento di Matematica, Università di Salerno e INFN Gruppo Collegato di Salerno, Via Giovanni Paolo II 132, 84084 Fisciano, Italy
[24] ISS, Atomistilor 409, 077125 Măgurele, Romania
[25] Institute of Physics/IHEF, University of Amsterdam, PO Box 94216, 1090 GE Amsterdam, The Netherlands
[26] TNO, Technical Sciences, PO Box 155, 2600 AD Delft, The Netherlands
[27] Dipartimento di Matematica e Fisica, Università degli Studi della Campania "Luigi Vanvitelli", viale Lincoln 5, 81100 Caserta, Italy
[28] Dipartimento di Fisica, Università La Sapienza, Piazzale Aldo Moro 2, 00185 Roma, Italy
[29] Dipartimento di Ingegneria dell'Energia Elettrica e dell'Informazione "Guglielmo Marconi", Università di Bologna, Via dell'Università 50, 47521 Cesena, Italia
[30] Physics Department, Faculty of Science Semlalia, Cadi Ayyad University, Av. My Abdellah, P.O.B. 2390, 40000 Marrakech, Morocco
[31] School of Physics, University of the Witwatersrand, Private Bag 3, Johannesburg Wits 2050, South Africa
[32] Dipartimento di Fisica e Astronomia "Ettore Majorana", Università di Catania, Via Santa Sofia 64, 95123 Catania, Italy
[33] INFN, LNF, Via Enrico Fermi, 40, 00044 Frascati, Italy
[34] INFN, Sezione di Bari, via Orabona, 4, 70125 Bari, Italy
[35] International Centre for Radio Astronomy Research, Curtin University, Bentley, WA 6102, Australia
[36] Subatech, IMT Atlantique, IN2P3-CNRS, Université de Nantes, 4 rue Alfred Kastler, La Chantrerie, BP 20722, 44307 Nantes, France
[37] Erlangen Centre for Astroparticle Physics, Friedrich-Alexander-Universität Erlangen-Nürnberg (FAU), Erwin-Rommel-Straße 1, 91058 Erlangen, Germany
[38] University Würzburg, Emil-Fischer-Straße 31, 97074 Würzburg, Germany
[39] School of Computing, Engineering and Mathematics, Western Sydney University, Locked Bag 1797, Penrith, NSW 2751, Australia
[40] Dipartimento di Fisica, Università di Salerno e INFN Gruppo Collegato di Salerno, Via Giovanni Paolo II 132, 84084 Fisciano, Italy
[41] IN2P3, LPC, Campus des Cézeaux 24, avenue des Landais, BP 80026, 63171 Aubière Cedex, France
[42] Università di Genova, Via Dodecaneso 33, 16146 Genova, Italy
[43] Dpto. de Física Teórica y del Cosmos, C.A.F.P.E., University of Granada, 18071 Granada, Spain
[44] NIOZ (Royal Netherlands Institute for Sea Research), PO Box 59, 1790 AB Den Burg Texel, The Netherlands
[45] Department of Physics, Tbilisi State University, 3, Chavchavadze Ave., 0179 Tbilisi, Georgia
[46] Leiden Institute of Physics, Leiden University, PO Box 9504, 2300 RA Leiden, The Netherlands
[47] National Centre for Nuclear Research, 02-093 Warsaw, Poland
[48] Institut Universitaire de France, 1 rue Descartes, 75005 Paris, France
[49] Physics Department, University La Sapienza, Roma, Piazzale Aldo Moro 2, 00185 Rome, Italy
[50] Department Physics, University of Johannesburg, PO Box 524, Auckland Park 2006, South Africa
[51] Laboratorio CIRCE, Dip. Di Matematica e Fisica, Università degli Studi della Campania "Luigi Vanvitelli", CAPACITY, Viale Carlo III di Borbone 153, 81020 San Nicola La Strada, Italy
[52] Dipartimento di Fisica, Università di Pisa, Largo Bruno Pontecorvo 3, 56127 Pisa, Italy
[53] School of Science and Technologies, The University of Georgia, Kostava str. 77, 0171 Tbilisi, Georgia
[54] Laboratoire Univers et Particules de Montpellier, Place Eugène Bataillon-CC 72, 34095 Montpellier Cédex 05, France
[55] Friedrich-Alexander-Universität Erlangen-Nürnberg (FAU), Remeis Sternwarte, Sternwartstraße 7, Bamberg 96049, Germany
[56] Université de Haute Alsace, rue des Frères Lumière, 68093 Mulhouse Cedex, France
[57] Institut für Kernphysik, University of Münster, Wilhelm-Klemm-Str. 9, 48149 Münster, Germany
[58] Department of Physics and Astronomy, Utrecht University, PO Box 80000, 3508 TA Utrecht, The Netherlands
[59] Centre for Cosmology, Particle Physics and Phenomenology, UCLouvain, Chemin du Cyclotron, 2, 1349 Louvain-la-Neuve, Belgium
[60] INFN, CNAF, v.le C. Berti-Pichat, 6/2, 40127 Bologna, Italy

Received: 18 November 2022 / Accepted: 14 March 2023 / Published online: 28 April 2023
© The Author(s) 2023

Abstract This article reports the first observation of the Moon and the Sun shadows in the sky distribution of cosmic-ray induced muons measured by the KM3NeT/ORCA detector. The analysed data-taking period spans from February 2020 to November 2021, when the detector had 6 Detection Units deployed at the bottom of the Mediterranean Sea, each composed of 18 Digital Optical Modules. The shadows induced by the Moon and the Sun were detected at their nominal position with a statistical significance of 4.2σ and 6.2σ, and an angular resolution of $\sigma_{res} = 0.49°$ and $\sigma_{res} = 0.66°$, respectively, consistent with the prediction of 0.53° from simulations. This early result confirms the effectiveness of the detector calibration, in time, position and orientation and the accuracy of the event direction reconstruction. This also demonstrates the performance and the competitiveness of the detector in terms of pointing accuracy and angular resolution.

Contents

1 Introduction

Cosmic rays (CR) are charged particles mainly composed of protons and light nuclei. Since they can be deflected by irregular Galactic magnetic fields, their arrival directions at the Earth are almost isotropic. Once a primary CR particle reaches the Earth's upper atmosphere and interacts with an air nucleus, it produces secondary particles. The most penetrating component of these are muons, which can be detected at the surface of the Earth but also at underground or underwater detectors. In order to reach the KM3NeT/ORCA detector [1] at a depth of 2500 ms below sea level [2], vertically downgoing muons need a minimal energy of around 500 GeV at sea level and thus they must have originated from primary CRs of energies exceeding several TeV/nucleon as described in [3]. 90% of the CR particles yielding muons used in this analysis have energies between 3 and 330 TeV as illustrated in Fig. 1. The angle between the primary CR and the secondary muon is on average within 0.1° at these energies [4] which is around 5 times lower than the expected angular resolution of the detector for muons. At the KM3NeT/ORCA detector the muons are dominantly minimal-ionizing with energies ranging from few tens of GeV to few hundred GeV.

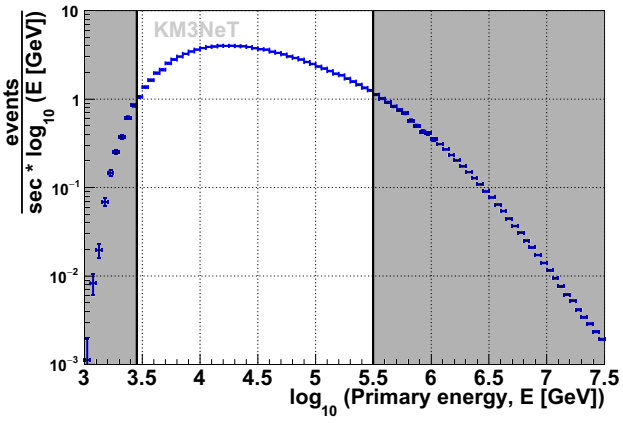

Fig. 1 Distribution of CR events which yield a reconstructed event in the KM3NeT/ORCA detector. The white region indicates the energy range which provides 90% of the event sample

CRs are blocked by nearby celestial bodies such as the Moon and the Sun. This induces a deficit in the atmospheric muon flux and in other secondary CR particles coming from the direction of these objects. This effect had been predicted by Clark in 1957 [5]. Its observation can be used to verify the pointing accuracy and angular resolution of detectors which are able to measure secondary particles from CR interactions. The Moon and the Sun shadows in CRs have been observed by multiple experiments (IceCube [6], ANTARES [7,8], MACRO [9], L3 [10], MINOS [11], ARGO-YBJ [12], HAWC [13] and others). As a permanent bright high-energy neutrino source has yet to be found, the observation of the Moon and Sun shadows in CRs is an important calibration tool for neutrino telescopes such as KM3NeT/ORCA and helps to demonstrate their pointing accuracy and to measure their angular resolution.

2 KM3NeT/ORCA detector

KM3NeT is a research infrastructure consisting of undersea Cherenkov neutrino telescopes currently under construction at the bottom of the Mediterranean Sea off-shore the Italian Sicily coast (KM3NeT/ARCA) and 40 km off-shore Toulon, France (KM3NeT/ORCA) [1]. The two detectors are optimised for different neutrino energy ranges. They are composed of vertical Detection Units (DUs). Six of them had been operational in KM3NeT/ORCA when the data used in this analysis were acquired. Each DU consists of 18 spherical Digital Optical Modules (DOMs), with 31 photomultiplier

[a] e-mail: brunner@cppm.in2p3.fr (corresponding author)
[b] e-mail: cerisy@cppm.in2p3.fr (corresponding author)

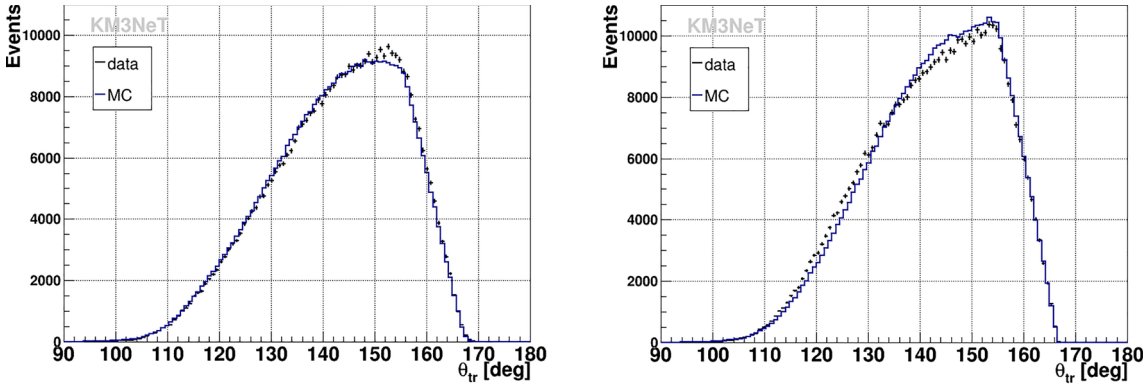

Fig. 2 Zenith angle distribution of selected events for the Moon (left) and the Sun (right). Data (black crosses) and simulations rescaled to data (blue histograms) are shown

tubes (PMTs) distributed almost isotropically within each DOM [14]. These PMTs detect the Cherenkov light emitted along the path of relativistic charged particles propagating through water. In the data acquisition a *hit* is produced when a photon impinging on a PMT induces an electrical signal above a defined threshold. A hit consists of a time stamp and a time over threshold. An event is created when the trigger algorithm identifies a series of causally-connected hits. For the analysis presented here, these events are processed by a track reconstruction algorithm. The hits are fitted with a model of a Cherenkov light emitting muon. This particle is assumed to follow a long, straight trajectory and to propagate practically at the speed of light in vacuum through water. The position, time and direction of such a track is determined by using a maximum-likelihood method based on a set of causally-connected hit times and positions [15]. A time-dependent calibration of the detector, with the monitored positions and orientations of every DOM computed and interpolated every 10 min, is used in this work to account for movements of the strings with the sea current.

3 Data and Monte Carlo samples

The data used in this analysis were collected between February 11, 2020, and November 18, 2021 for a total of 499.3 days. Quality cuts on the number of used hits and the likelihood of the track reconstruction were applied to remove poorly reconstructed events keeping 83% of the initial event sample. An average event density of 3000 events per square degree is measured in the vicinity of Moon and Sun. It is expected that about 640 CR events are blocked by each of the two sky objects. The position of the Moon/Sun in the sky is obtained using the *astropy* package [16] that relies on the International Celestial Reference System (ICRS) coordinates described in [17]. The latitude of 43° North of the detector and the data taking period of more than one year lead to broad zenith angle distributions of the selected events in the vicinity of Sun and Moon as shown in Fig. 2.

Monte Carlo (MC) simulations are used to optimise the track selection, and predict the angular resolution and amplitude of the CR deficit induced by the Moon and the Sun. Secondary muons at the KM3NeT/ORCA detector are simulated with the MUPAGE package [18,19]. These muons are then propagated through sea water and Cherenkov photons are created within a cylindrical volume surrounding the simulated detector. Finally the detector response is simulated by producing digitized hits from photons detected by PMTs and by adding noise hits from environmental background mainly due to ^{40}K decay and bioluminescence. These are derived from real data runs in a time-dependent way following the *run-by-run* approach previously introduced by the ANTARES Collaboration [3]. The time-dependent PMT efficiencies are monitored and used in the simulation. The last two steps are done with KM3NeT custom software [15]. The resulting hit patterns are passed through the trigger and reconstruction steps using the same software that is used to process real data. The simulated track sample is about 4 times larger compared to the real data sample.

The optimisation of the track selection is performed by varying the cut on the angular error estimate from the track reconstruction to maximize the significance of the shadow signal. By requiring a more and more stringent cut a smaller but higher quality event sample is selected. The chosen value keeps 45% of the original MC sample.

4 Analysis method

The search for the shadow of the Moon/Sun is done in the phase space of the angular differences between the reconstructed track coordinates and the celestial object. Both a 1-dimensional and a 2-dimensional analysis have been performed. The 1-dimensional analysis uses the space angle

between the direction of the Moon/Sun and the track. The 2-dimensional analysis uses two Cartesian coordinates (x, y), starting from the zenith and azimuth angles of the sky object θ_{sk}, α_{sk} and the tracks θ_{tr}, α_{tr} respectively,

$$\begin{aligned} x &= (\alpha_{sk} - \alpha_{tr}) \sin\theta_{tr} \\ y &= \theta_{sk} - \theta_{tr} \end{aligned} \tag{1}$$

2D maps that extend to $\pm 6^\circ$ in (x, y) have been constructed. Data are only used for times when the full $\pm 6^\circ$ field around the Moon/Sun is above the horizon. An angular range of $\pm 6^\circ$ contains the detectable shadow signal entirely and it allows for a simultaneous fit of the shadow and background parameters while analysing just a moderately-sized atmospheric muon sample. It has been verified that the results do not depend on the precise choice of the chosen angular range. A constant 0.1° binning in x and y is chosen, however results are reproduced when choosing a smaller binning. The 1D histogram contains tracks that are closer than 4° to the Moon/Sun position.

The significance of the shadowing effect of Moon/Sun is determined with a likelihood ratio test, by comparing the likelihood of a background hypothesis model H_0, with the likelihood of a signal plus background model H_1 which includes a shadowing effect. The Poisson likelihood with the definition in Ref. [20]

$$\chi^2(H) = 2\sum_{i}^{N_{bin}} [N_{i,H} - n_i + n_i \ln(n_i/N_{i,H})] \tag{2}$$

is used, where n_i stands for the event count in the i-th space angle bin to be compared with the expectations $N_{i,H}$ under the H_0 and H_1 hypotheses. The difference in $\Delta\chi^2_{H1/H0} = \chi^2(H_1) - \chi^2(H_0)$ values is used to determine the probability to reject the null hypothesis and to extract the significance of the observation from it. The background event distribution in azimuth is found to be uniform, while the zenith angle dependency can be conveniently parametrized with a 2^{nd} order polynomial function. This yields for the 2D maps

$$N_{i,H_0} = \rho\left[1 + a_1 y_i + a_2 y_i^2\right] \tag{3}$$

with ρ a constant track density per space angle and a_1, a_2 parameters which are determined during minimisation. For the 1D maps, each bin contains events from an almost symmetric zenith angle range above and below the Moon/Sun position resulting in a uniform exposure, i.e. $N_{i,H_0} = \rho$.

The event expectation in bin i for the signal plus background hypothesis H_1 is defined as

$$N_{i,H_1} = N_{i,H_0} - \rho \cdot G_i \tag{4}$$

where G_i describes the deficit of secondary CR events due to the shadowing effects of Moon/Sun in bin i with coordinates x_i, y_i as a bi-dimensional Gaussian

$$\begin{aligned} &G_i(A, \sigma_{res}, x_s, y_s) \\ &= A\frac{R_s^2}{2\sigma_{res}^2} \exp\left[-\frac{(x_i - x_s)^2 + (y_i - y_s)^2}{2\sigma_{res}^2}\right] \end{aligned} \tag{5}$$

where A is the relative shadow amplitude. For $A = 1$ the number of blocked CR events correspond to $\rho\pi R_s^2$. The angular resolution of the detector for the selected sample of CR events is measured by σ_{res}, the angular width of the Gaussian shadow. The R_s, x_s, y_s parameters are the apparent angular radius of the celestial object and the relative angular position of the Moon/Sun shadow with respect to their nominal positions. For the 1D maps, the term $(x_i - x_s)^2 + (y_i - y_s)^2$ in Eq. (5) is replaced by δ^2, the square of the angular distance between the track and the sky object from Eq. (6) with V_{tr} and V_{sk} the direction vector of the track and the sky object respectively.

$$\delta = \arccos(V_{tr} \cdot V_{sk}) * 180/\pi \tag{6}$$

The significance of the shadow is found by fitting ρ, a_1, a_2, A and σ_{res} at $(x_s, y_s) = (0, 0)$ on the 2D or 1D event distribution respectively. Results from these fits are summarized in Sect. 5.2. The position of the shadow is obtained by simultaneously fitting $\rho, a_1, a_2, (x_s, y_s)$ and A, with σ_{res} fixed to its expectation value from MC. Results from these fits are found in Sect. 5.3.

The assumption of Gaussianity of the shadowing effect is the result of a few approximations. Firstly, the influence of the size of the Moon/Sun is neglected. This is acceptable as long as the angular resolution of the detector is larger than the angular radius of the Moon/Sun, a condition which is amply satisfied in the present case. In addition, the real point spread function (PSF) of the detector has a slightly different radial shape compared to a Gaussian function (see Fig. 3, right) which will be accounted for by fitting the shadow amplitude A when comparing data to the H_1 hypothesis. It is observed, that the PSF is identical for the data samples selected for Moon and Sun.

Further, the PSF is perfectly symmetric in x and y as shown in Fig. 3 (left), allowing for a reliable fit of x_s and y_s.

The Moon radius varies between 0.245° and 0.279° resulting in an amplitude variation of $\pm 14\%$ around the mean value. However our data sample covers several Moon cycles, so the average value is used. A similar statement can be made for the Sun whose apparent radius varies between 0.262° and 0.271° during the year.

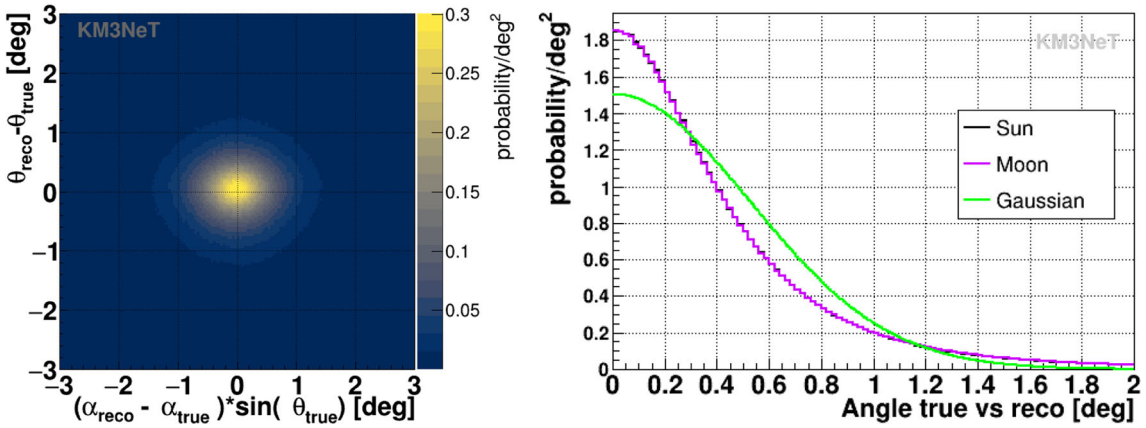

Fig. 3 PSF from MC, i.e. the difference between the true muon direction and the reconstructed one in 2-dimensional angular space (left) and as function of the space angle difference (right, blue and magenta for Sun and Moon, respectively). A Gaussian PSF with $\sigma = 0.53°$ is shown in green for comparison

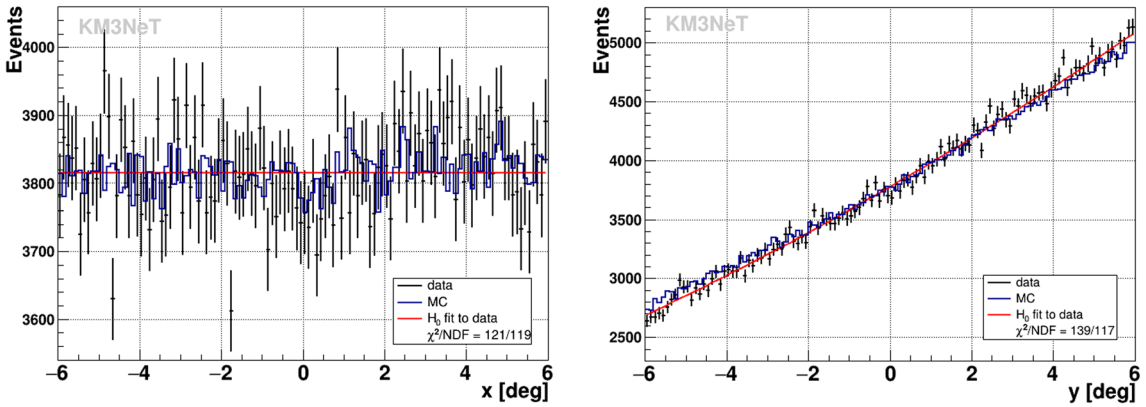

Fig. 4 Event distribution in x and y for the Sun data sample (black crosses) compared to the polynomial fits from the H_0 hypothesis (red lines) and MC predictions rescaled to data (blue histograms)

5 Data analyses

5.1 Background

The background distributions in x and y are shown in Fig. 4 for the Sun as an example. Fits of the H_0 hypothesis using a constant, and 2^{nd} order polynomial function describe the data well. The MC predictions are also compatible with these functions.

5.2 Fits at nominal positions

Figure 5 shows the 1D distributions of the event density as a function of the angular distance from the Moon/Sun. The fit results from the 1D and 2D fits at $(x_s, y_s) = (0, 0)$ are summarized in Table 1. The significances are derived from the $\Delta\chi^2_{H1/H0}$ with two degrees of freedom (A, σ_{res}). The values obtained for A and σ_{res} can be compared to MC expectations of $A = 0.90 \pm 0.09$ and $\sigma_{res} = (0.53 \pm 0.04)°$ for the combined Moon/Sun sample. The fitted values of σ_{res} are found compatible with the prediction from simulations. The deeper amplitude and higher significance of the Sun shadow is consistent with the effects of the particular structure of the Sun's magnetic field during the periods of low solar activity, whose dipole shape is expected to enhance the Sun shadowing effect [21].

5.3 Positional fits

The results from the fits of the 2D map in (x_s, y_s) with $\sigma_{res} = 0.53°$ are shown in Fig. 6. The plot illustrates $\chi^2(H_1) - \chi^2(H_0)$ in colour coding. The image of the shadow is clearly visible. Figure 7 shows the 1σ (68.3%), 2σ (95.4%), 3σ (99.7%) confidence contours for the two parameters (x_s, y_s) around the best fit point $x_s = (0.11 \pm 0.21)°$, $y_s = (0.04 \pm 0.13)°$ for the Moon and $x_s = (-0.01 \pm 0.11)°$, $y_s = (0.10 \pm 0.12)°$ for the Sun. The true position of the Moon and the Sun in Fig. 7 are contained within the 68%

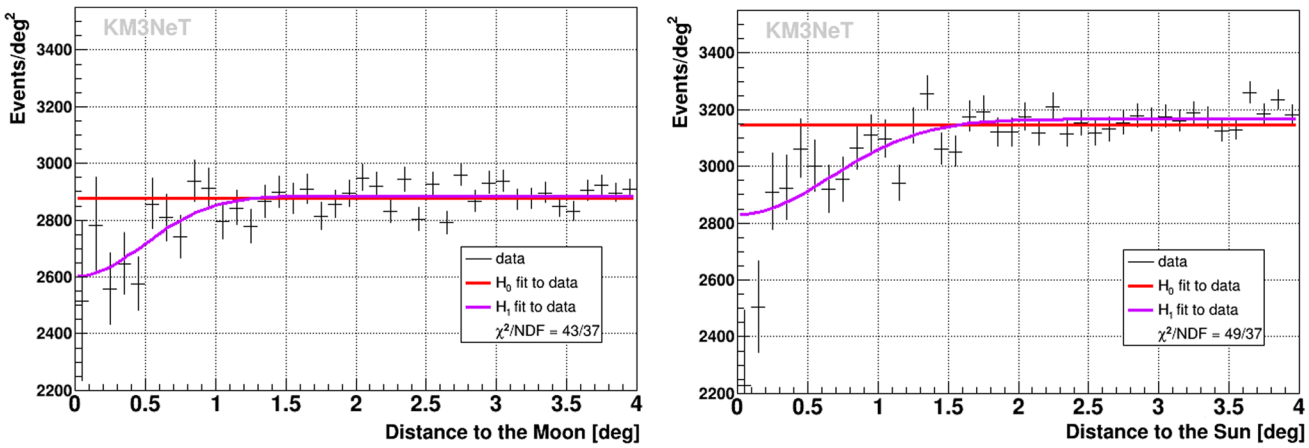

Fig. 5 Event density as a function of the distance to the Moon on the left and the Sun on the right. Data (black crosses) are compared to the H_0 fit (red) and the H_1 fit (magenta)

Table 1 Parameters from the fits at nominal position $(x_s, y_s) = (0, 0)$

Parameters	Moon 1D	Moon 2D	Sun 1D	Sun 2D
σ_{res}	$0.49° \pm 0.11°$	$0.49° \pm 0.15°$	$0.66° \pm 0.08°$	$0.65° \pm 0.13°$
A	0.69 ± 0.17	0.71 ± 0.27	1.38 ± 0.31	1.31 ± 0.34
$\Delta\chi^2_{H1/H0}$	-20.7	-21.3	-47.2	-43.0
Significance	4.2σ	4.2σ	6.5σ	6.2σ
Events/deg^2	2886	2892	3166	3161

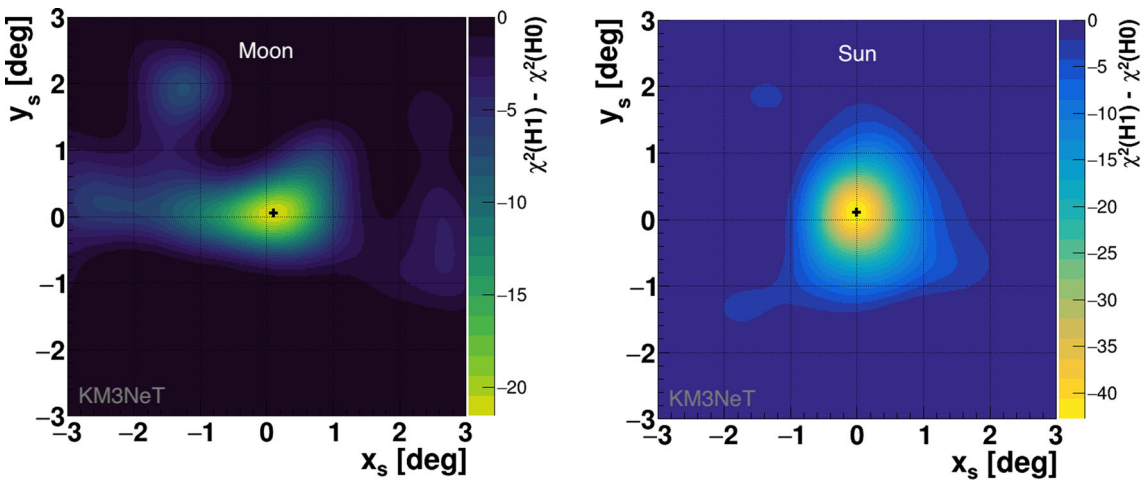

Fig. 6 Colour-coded $\Delta\chi^2_{H1/H0}$ as a function of x_s and y_s for the Moon (left) and the Sun (right)

contours, yielding a 84% and 67% compatibility between the nominal and the best fit positions, calculated from the corresponding $\Delta\chi^2$ with two degrees of freedom (x_s, y_s). The slightly different shapes of the contours for Moon and Sun can be entirely attributed to statistical fluctuations.

6 Conclusion

The Moon and the Sun's CR shadows have been observed with a high statistical significance using data collected between February 2020 and November 2021 with 6 Detection Units of the KM3NeT/ORCA detector. The demonstrated sensitivity to the shadow observation with only one and half years of data taking and a yet incomplete detector reflects

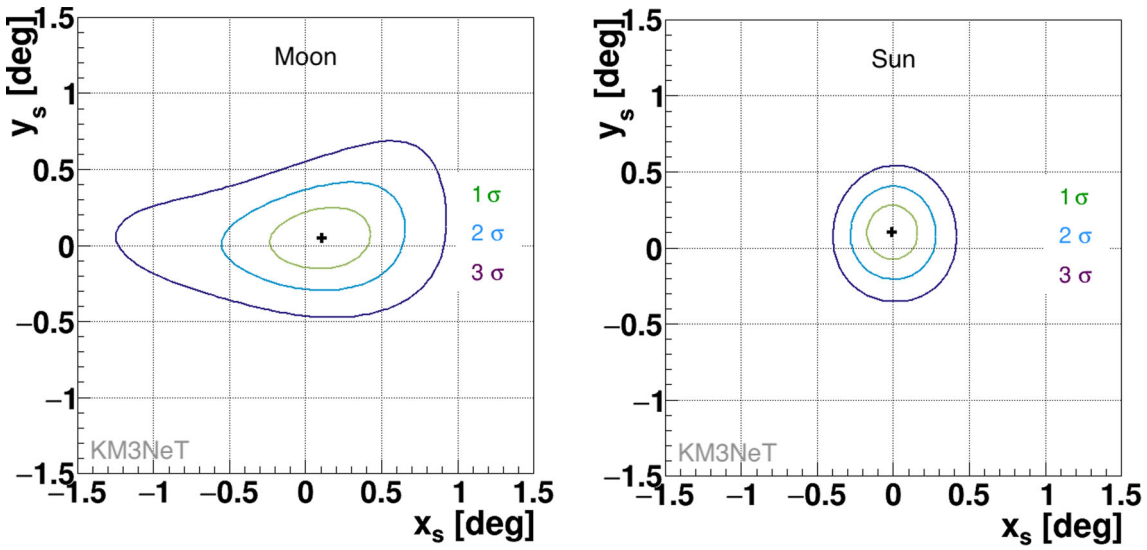

Fig. 7 Confidence intervals derived from Fig. 6 for the Moon (left) and the Sun (right). The black cross indicates the best fit point

the good understanding of the detector positioning, orientation, time calibration [22] and reconstruction capabilities. The shadow observed in data is compatible with expectations from MC concerning the significance, angular width and amplitude, except for the Sun's amplitude, where it was found above expectations.

Acknowledgements The authors acknowledge the financial support of the funding agencies: Agence Nationale de la Recherche (contract ANR-15-CE31-0020), Centre National de la Recherche Scientifique (CNRS), Commission Européenne (FEDER fund and Marie Curie Program), Institut Universitaire de France (IUF), LabEx UnivEarthS (ANR-10-LABX-0023 and ANR-18-IDEX-0001), Paris Île-de-France Region, France; Deutsche Forschungsgemeinschaft (DFG), Germany; The General Secretariat of Research and Technology (GSRT), Greece; Istituto Nazionale di Fisica Nucleare (INFN), Ministero dell'Università e della Ricerca (MIUR), PRIN 2017 program (Grant NAT-NET 2017W4HA7S) Italy; Ministry of Higher Education, Scientific Research and Innovation, Morocco, and the Arab Fund for Economic and Social Development, Kuwait; Nederlandse organisatie voor Wetenschappelijk Onderzoek (NWO), the Netherlands; The National Science Centre, Poland (2021/41/N/ST2/01177); National Authority for Scientific Research (ANCS), Romania; Grants PID2021-124591NB-C41, -C42, -C43 funded by MCIN/AEI/ 10.13039/501100011033 and, as appropriate, by "ERDF A way of making Europe", by the "European Union" or by the "European Union NextGenerationEU/PRTR", Programa de Planes Complementarios I+D+I (refs. ASFAE/2022/023, ASFAE/2022/014), Programa Prometeo (PROMETEO/2020/019) and GenT (refs. CIDEGENT/2018/034, /2019/043, /2020/049. /2021/23) of the Generalitat Valenciana, Junta de Andalucía (ref. SOMM17/6104/UGR, P18-FR-5057), EU: MSC program (ref. 101025085), Programa María Zambrano (Spanish Ministry of Universities, funded by the European Union, NextGenerationEU), Spain.

Data Availability Statement This manuscript has no associated data or the data will not be deposited. [Authors' comment: The public data will be published according to KM3NeT open science politics.]

Open Access This article is licensed under a Creative Commons Attribution 4.0 International License, which permits use, sharing, adaptation, distribution and reproduction in any medium or format, as long as you give appropriate credit to the original author(s) and the source, provide a link to the Creative Commons licence, and indicate if changes were made. The images or other third party material in this article are included in the article's Creative Commons licence, unless indicated otherwise in a credit line to the material. If material is not included in the article's Creative Commons licence and your intended use is not permitted by statutory regulation or exceeds the permitted use, you will need to obtain permission directly from the copyright holder. To view a copy of this licence, visit http://creativecommons.org/licenses/by/4.0/.

Funded by SCOAP[3]. SCOAP[3] supports the goals of the International Year of Basic Sciences for Sustainable Development.

References

1. S. Adrián-Martínez et al., J. Phys. G Nucl. Part. Phys. **43**(8), 084001 (2016). https://doi.org/10.1088/0954-3899/43/8/084001
2. M. Ageron et al., Eur. Phys. J. C **80**(2), 99 (2020). https://doi.org/10.1140/epjc/s10052-020-7629-z
3. A. Albert et al., J. C. A. P. **2021**(01), 064 (2021). https://doi.org/10.1088/1475-7516/2021/01/064
4. R. Abbasi et al., Phys. Rev. D **87**(1), 012005 (2013). https://doi.org/10.1103/PhysRevD.87.012005
5. G.W. Clark, Phys. Rev. D **108**(2), 450 (1957). https://doi.org/10.1103/PhysRev.108.450
6. M. Aartsen et al., Phys. Rev. D **103**(4), 042005 (2021). https://doi.org/10.1103/PhysRevD.103.042005
7. A. Albert et al., Eur. Phys. J. C **78**(12), 1006 (2018). https://doi.org/10.1140/epjc/s10052-018-6451-3
8. A. Albert et al., Phys. Rev. D **102**(12), 122007 (2020). https://doi.org/10.1103/PhysRevD.102.122007
9. M. Ambrosio et al., Astropart. Phys. **20**(2), 145 (2003). https://doi.org/10.1016/S0927-6505(03)00169-5
10. P. Achard et al., Astropart. Phys. **23**(4), 411 (2005). https://doi.org/10.1016/j.astropartphys.2005.02.002
11. P. Adamson et al., Astropart. Phys. **34**(6), 457 (2011). https://doi.org/10.1016/j.astropartphys.2010.10.010

12. B. Bartoli et al., Phys. Rev. D **84**(2), 022003 (2011). https://doi.org/10.1103/PhysRevD.84.022003
13. A.U. Abeysekara et al., Proc. 33rd ICRC, Rio de Janeiro (2013). arXiv:1310.0072
14. S. Aiello et al., J. Instrum. **17**(07), P07038 (2022). https://doi.org/10.1088/1748-0221/17/07/P07038
15. K. Melis, A. Heijboer, M. De Jong et al., Proc. 35th ICRC, p. 950 (2017). https://doi.org/10.22323/1.301.0950
16. A.M. Price-Whelan et al., Astron. J. **156**(3), 123 (2018). https://doi.org/10.3847/1538-3881/aabc4f
17. F. Arias, P. Charlot, M. Feissel, J. Lestrade, Astron. Astrophys. **303**, 604 (1995)
18. G. Carminati, M. Bazzotti, A. Margiotta, M. Spurio, Comput. Phys. Commun. **179**(12), 915 (2008). https://doi.org/10.1016/j.cpc.2008.07.014
19. Y. Becherini, A. Margiotta, M. Sioli, M. Spurio, Astropart. Phys. **25**(1), 1 (2006). https://doi.org/10.1016/j.astropartphys.2005.10.005
20. S. Baker, R.D. Cousins, Nucl. Instrum. Meth. **221**(2), 437 (1984). https://doi.org/10.1016/0167-5087(84)90016-4
21. J. Becker Tjus, P. Desiati, N. Döpper, H. Fichtner, J. Kleimann, M. Kroll, F. Tenholt, A.&A. **633**, A83 (2020). https://doi.org/10.1051/0004-6361/201936306
22. R. Coniglione, A. Creusot, I. Di Palma, D. Guderian, J. Hofestaedt, G. Riccobene, A. Sánchez-Losa, Proc. 36th ICRC, ICRC2019, 868 (2019). https://doi.org/10.22323/1.358.0868